ATLAS Internal Note
CAL-NO-063
15 December 94

# The Jet Energy Resolution of the End-Cap Calorimeter of ATLAS

A.E. Kiryunin

Institute for High Energy Physics
Protvino, 142284 Moscow region, Russia

**Abstract**

The energy resolution of jets in the liquid argon end-cap calorimeter of ATLAS in the configuration with and without a preshower has been studied. The dependence of the resolution on the jet cone size has also been investigated. The studies are based on detailed Monte Carlo simulations.

The ATLAS detector has a liquid argon (LAr) calorimeter in the end-cap region. It consists of three parts: a hadronic calorimeter, an electromagnetic calorimeter and (optionally) a cold preshower. The goal of this work is to estimate the energy resolution of jets, which can be achieved in this set-up as function of boths, jet energy and jet size.

# 1 Simulation Procedure

Studies of the energy resolution of jets in the ATLAS end-cap calorimeter are based on detailed Monte Carlo simulations.

Single d-quark jets are generated with the PYTHIA 5.7 program [1] at a pseudorapidity $\eta = 2.45$ at six energy points: 40, 100, 200, 500, 1000 and 2000 GeV. This corresponds to transverse energies of 7, 17, 34, 86, 171 and 343 GeV respectively. The number of jets per energy point is 1000. The energy distribution of jets is shown in Fig. 1.

Simulations are done in the framework of the standard ATLAS software DICE/SLUG. For the end-cap calorimeters the geometry version 2 is taken:

- hadronic LAr calorimeter (ENDH) with $\eta$-coverage up to 3.3,
- electromagnetic LAr calorimeter (ENDE) with $\eta$-coverage up to 3.1,
- cold preshower (COPE) with $\eta$-coverage up to 2.7.

For the inner tracker the so-called "panel" geometry version is used. The distribution of material (in absorbtion lengths $\lambda_{abs}$) in the end-cap region as function of the pseudorapidity is shown in Fig. 2.

The detector response to the final state particles from jets is simulated using the program GEANT 3.21 [2] with the FLUKA code for shower development.

# 2 Analyzing Procedure

In Fig. 3 the distributions of the energy, deposited in the hadronic and electromagnetic calorimeters and in the preshower (in the region $1.5 \leq \eta \leq 3.3$), are shown for different values of the initial jet energy. To switch from the deposited energy scale to the jet energy scale, calibration constants should be applied for the different parts of the calorimeter.

To determine these calibration constants, a standard procedure, which minimizes the energy resolution with respect to the generated jet energy, is applied. The reconstructed jet energy in the $i^{th}$ event is defined as

$$E_i = \sum_{j=1}^{M} C_j \cdot E_{ij},$$

where $E_{ij}$ — energy deposited in $j^{th}$ part of the calorimeter in the $i^{th}$ event, $C_j$ — calibration constants, $M$ — number of parts of the calorimeter with different calibration constants. Calibration constants are determined by minimizing the following functional

$$F = \sum_{i=1}^{N} (E_i - E_i^{jet})^2,$$

where $E_i^{jet}$ — energy of a jet in the $i^{th}$ event, $N$ — number of events.

The studies are done for two configurations of the end-cap calorimeter of ATLAS: without and with a preshower. For the first configuration only energy depositions in the hadronic and electromagnetic calorimeters are taken into account, using two calibration constants (defined as mentioned above). For the second configuration the energy, deposited in the preshower, is also considered, and three calibration constants are used. It should be stressed, that neither longitudinal nor transverse structure of the end-cap calorimeters are used in this procedure, therefore only one calibration constant per calorimeter/preshower is applied.

The energy dependence of the calibration constants, determined after two parameter minimization (for the configuration without a preshower) and after three parameter minimization (for the configuration with a preshower), is shown in Fig. 4. This dependence is rather weak.

The resulting energy distributions after applying two or three calibration constants are shown in Fig. 5 and Fig. 6 respectively for different values of the initial energy of jets. To determine the energy resolution, Gaussian curves are fitted to these energy distributions in an interval of $\pm 3\sigma$ around the peak value. The mean value $E$ and the standard deviation $\sigma$ from this fit are used to calculate the resolution $\sigma/E$.

The matter of interest is not the energy resolution in the total volume of end-cap calorimeters, but the energy resolution using a limited space in pseudorapidity $\eta$ and azimuthal angle $\varphi$, as determined from jet finding. For the present studies the following jet finding algorythm is used: The reconstructed energy, defined after applying the calibration constants (determined once for the total volume of end-cap calorimeters), is stored in a $18\times64$ matrix. This matrix covers the end-cap volume ($1.5 \leq \eta \leq 3.3$ and full azimuthal range). Its granularity equals to the transverse granularity of the hadronic end-cap calorimeter of $\Delta\eta \times \Delta\varphi = 0.1 \times 2\pi/64$. In each event a jet axis as a coordinate $(\eta_0, \varphi_0)$ is found by using a simple clustering algorythm. The energy of the jet is detemined by summing energies of all cells with coordinates inside a circle with the centre $(\eta_0, \varphi_0)$ and the radius $R = \sqrt{(\eta - \eta_0)^2 + (\varphi - \varphi_0)^2}$. The radius $R$ is a measure of the jet cone size accepted.

# 3 Results and Conclusions

In Fig. 7 the energy resolution as a function of the variable $1/\sqrt{E_{JET}}$ is shown for different volumes (the end-cap volume and the volume of jets with different sizes $R$). The data shown are obtained with the two parameter minimization approach. The energy dependence of the resolution is fitted by a linear sum with two terms:

$$\frac{\sigma}{E} = \frac{A}{\sqrt{E_{JET}}} + B, \tag{1}$$

with a sampling term $A$ and a constant term $B$. The results of the fit are plotted in Fig. 7 as straight lines and printed in the right top corner of the corresponding plots.

The results of the fit show, that the parameterization (1) describes the energy dependence of the resolution rather badly. The largest difference between data and fitted line is at small jet energies: 40 and 100 GeV. Such a degradation of the energy resolution can be understood considering the following arguments: At first, the average energies of hadrons in 40 and 100 GeV jets are rather small: about 5 and 10 GeV respectively and the jet cone is rather wide. At second, the thickness of materials of the inner tracker and cryostat walls in front of the end-cap calorimeter is at least 0.5 $\lambda$ (see Fig. 2). Energy losses there, should lead to the degradation of the energy resolution.

To take into account these energy losses in front of the end-cap calorimeter one more term,the so-called material term, which is independent of energy, can be added quadratically to (1):

$$\frac{\sigma}{E} = \left(\frac{A}{\sqrt{E_{JET}}} + B\right) \oplus \frac{C}{E_{JET}}, \tag{2}$$

where $C$ is a material term. The results of the fit (2) are shown in Fig. 7 as curves and printed below the results of the fit by the (1). The ansatz (2) describes the energy dependence of the resolution for all jet cones considered well.

The analysis of the energy dependence of the resolution, obtained with the usage of the calibration procedure with three parameter minimization (see Fig. 8), leads to the same conclusion.

In Fig. 9 the sampling, constant and material terms, obtained by fitting the ansatz (2) to the energy dependence of the resolution of jets for the configurations of the end-cap calorimeter with and without a preshower, are plotted as function of the jet cone size considered. The sampling term practically does not depend on the jet cone size in the range above $R$=0.6 for both configurations. The constant term increases slightly with decreasing jet cone size. But the most significant dependence is observed for the material term. It degrades by a factor 3.5, if one compares results for the total end-cap volume and for jet cone size with $R$=0.5. This means, that this term takes into account not only the energy losses due to the material in front of the calorimeter, but also the lateral energy losses due to the finite jet cone size.

The main difference between the configurations of the end-cap calorimeter with and without a preshower is in the sampling term. For the total end-cap volume this term (31±2)% and (40±3)% $GeV^{1/2}$ respectively. For a jet cone size $R$=0.7 (which is appropriate for the jet spectroscopy under the LHC conditions) these values are (31±5)% and (38±5)% $GeV^{1/2}$ respectively. This result shows, that the information concerning the energy deposited in a thin layer of LAr in the front of the electromagnetic calorimeter can improve the energy resolution of jets significantly.

In conclusion, the Table 1 summarizes the main results of the studies.

| | Presence of a preshower | |
|---|---|---|
| | No | Yes |
| $A\ [\%\sqrt{GeV}]$ | 38 ± 5 | 31 ± 5 |
| $B$ [%] | 0.9 ± 0.1 | 0.7 ± 0.1 |
| $C$ [$GeV$] | 5.2 ± 0.3 | 5.0 ± 0.3 |
| $\chi^2/NDF$ | 0.7 | 0.5 |

Table 1: The results of the fit of the energy dependence of the resolution using the three term ansatz (2) for a jet cone size of $R$=0.7.

# References

[1] T. Sjöstrand CERN-TH.7112/93 (1994).

[2] R. Brun et al., GEANT3, CERN Program Library Writeup W5013.

*

# List of Figures

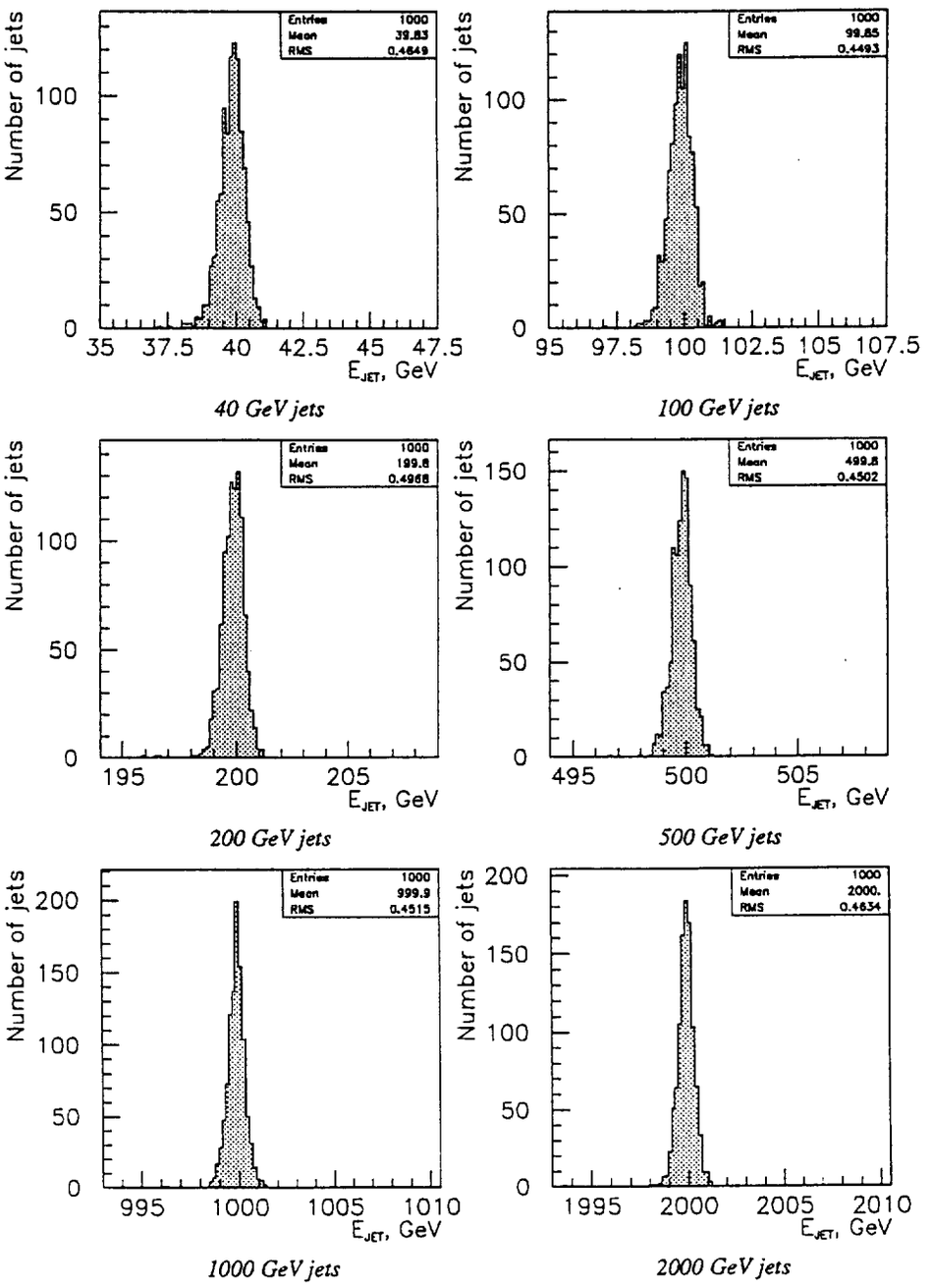


Figure 1: The jet energy distribution.

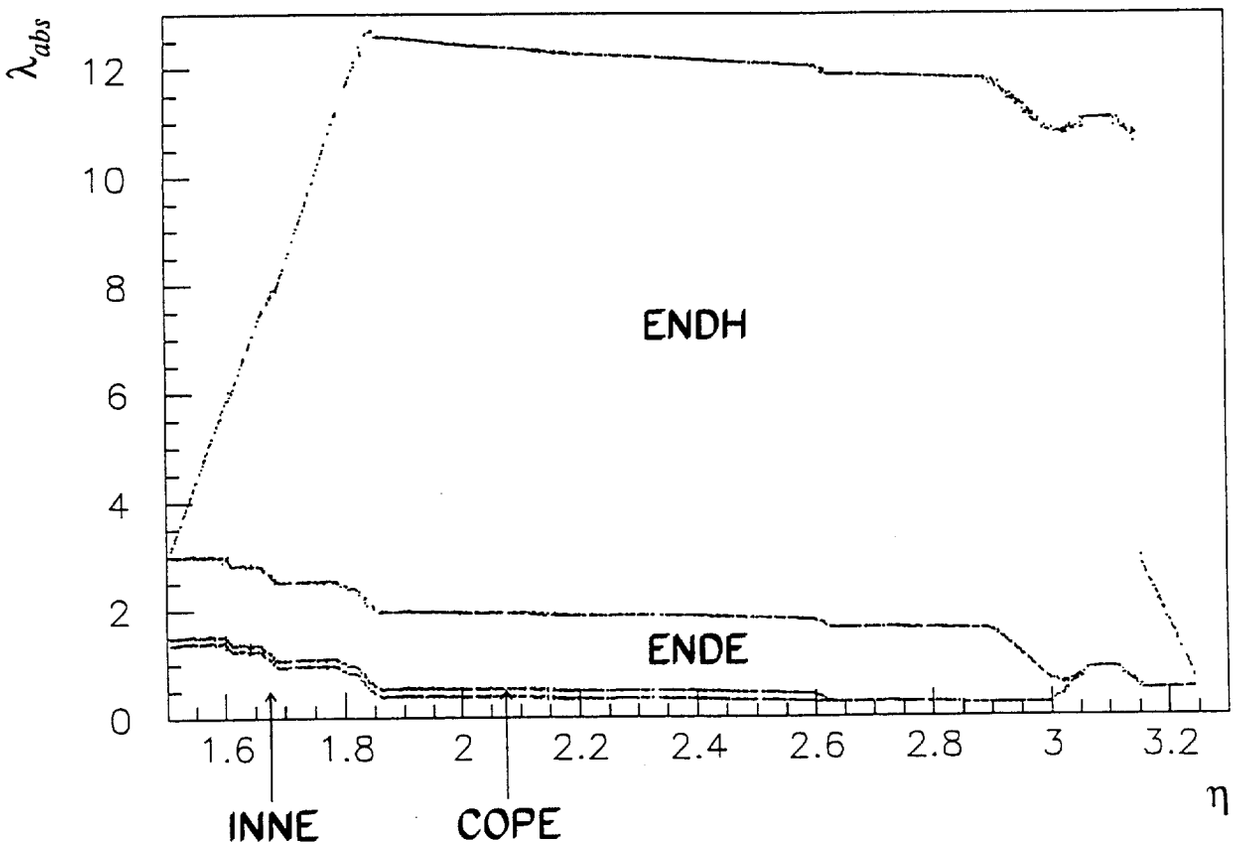


Figure 2: The distribution of material in the end-cap region as function of the pseudorapidity (ENDH — hadronic calorimeter, ENDE — electromagnetic calorimeter, COPE — cold preshower, INNE — inner tracker and cryostat).

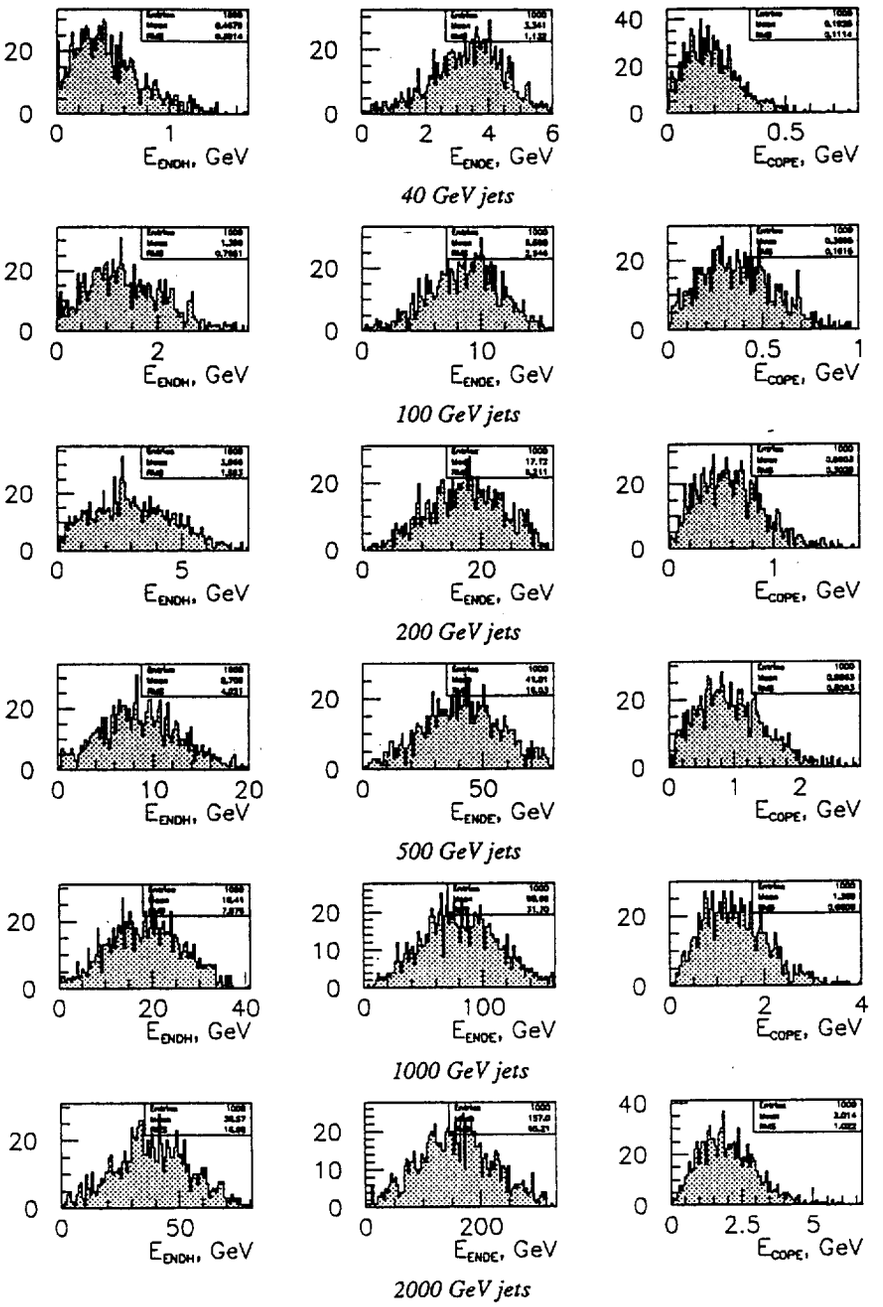


Figure 3: The distributions of the deposited energy.

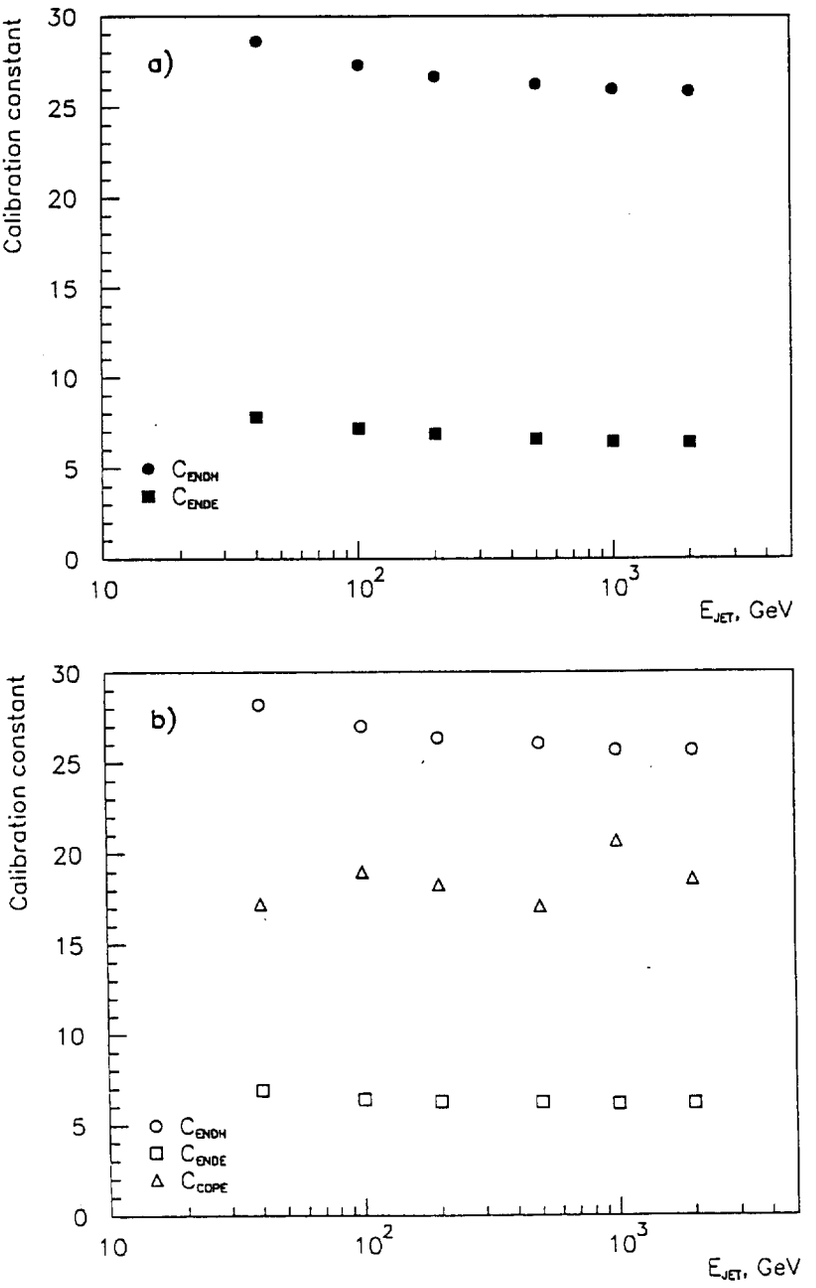


Figure 4: The energy dependence of the calibration constants for the configuration without a preshower (a) and with a preshower (b).

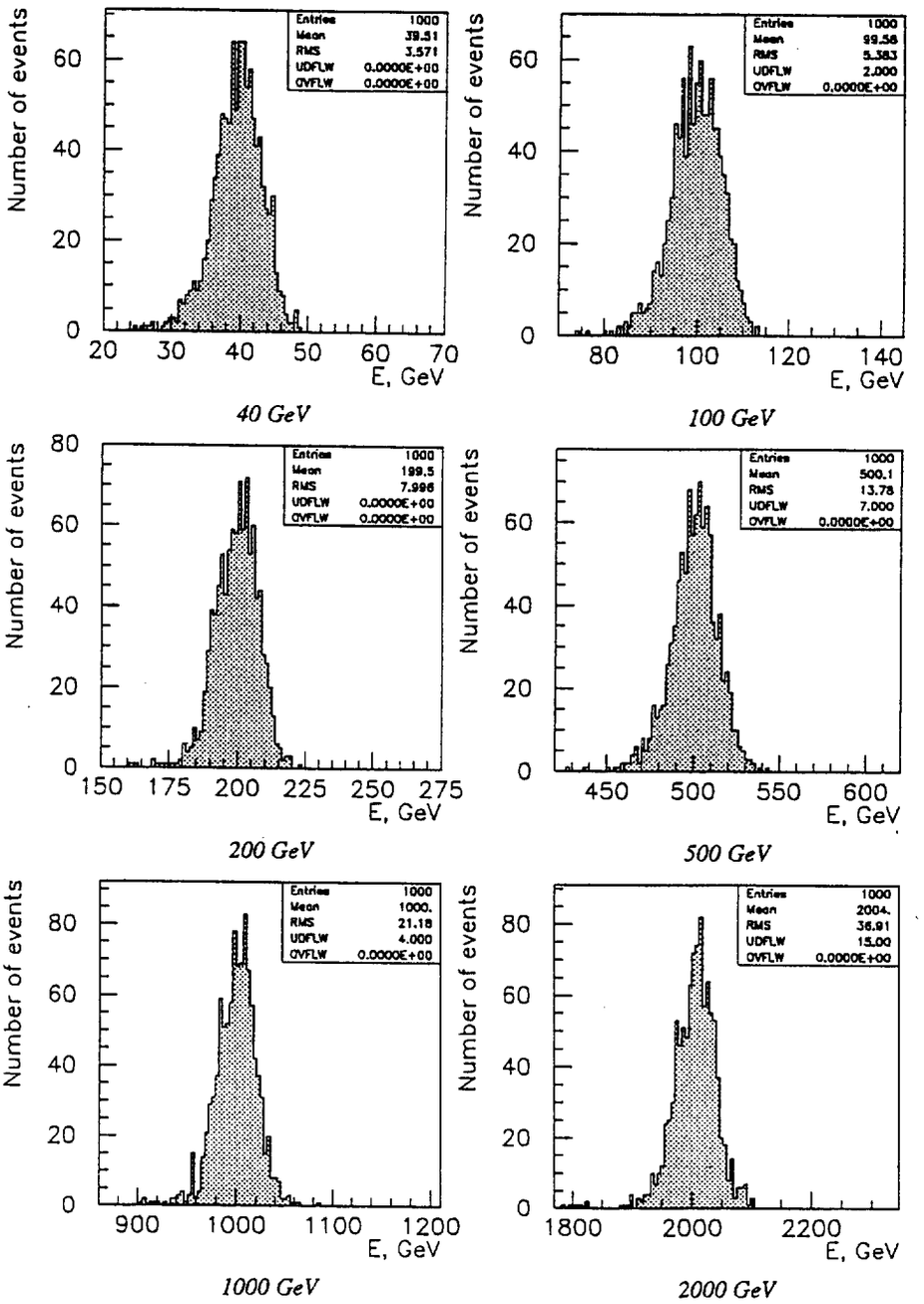


Figure 5: The distributions of reconstructed energy for the configuration without a preshower (after two parameter minimization).

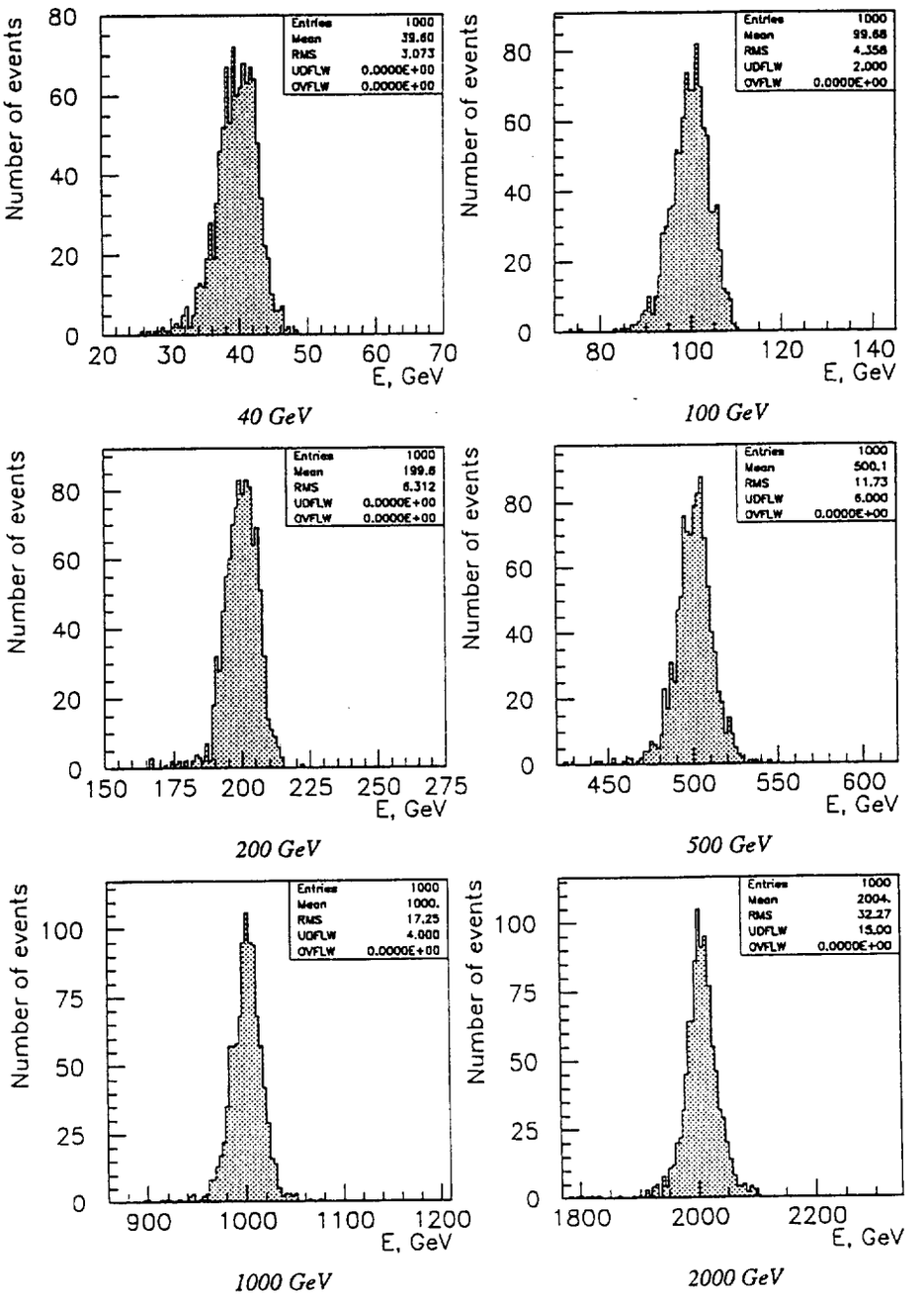


Figure 6: The distributions of reconstructed energy for the configuration with a preshower (after three parameter minimization).

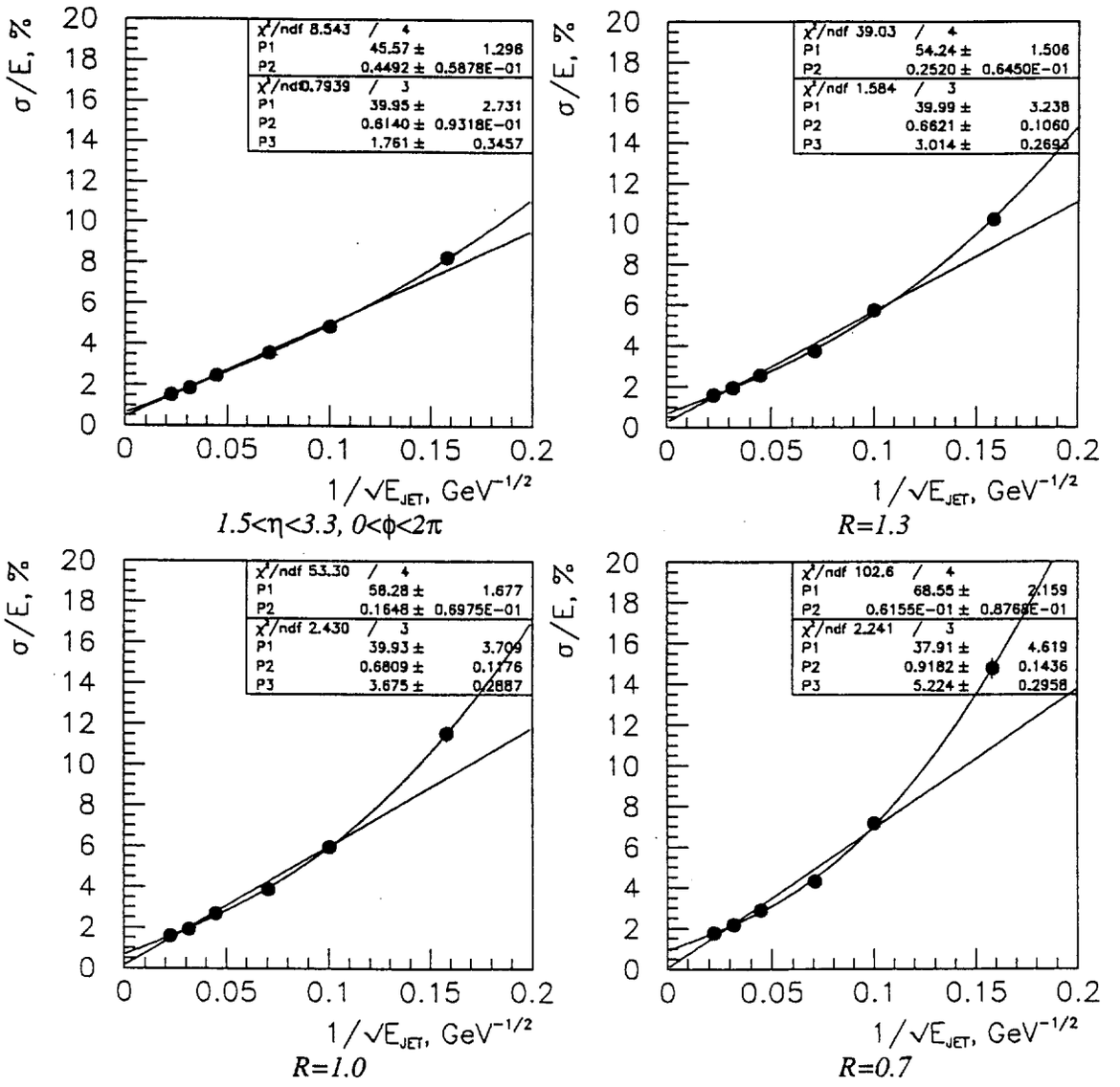


Figure 7: The energy dependence of the resolution for the configuration without a preshower (after two parameter minimization).

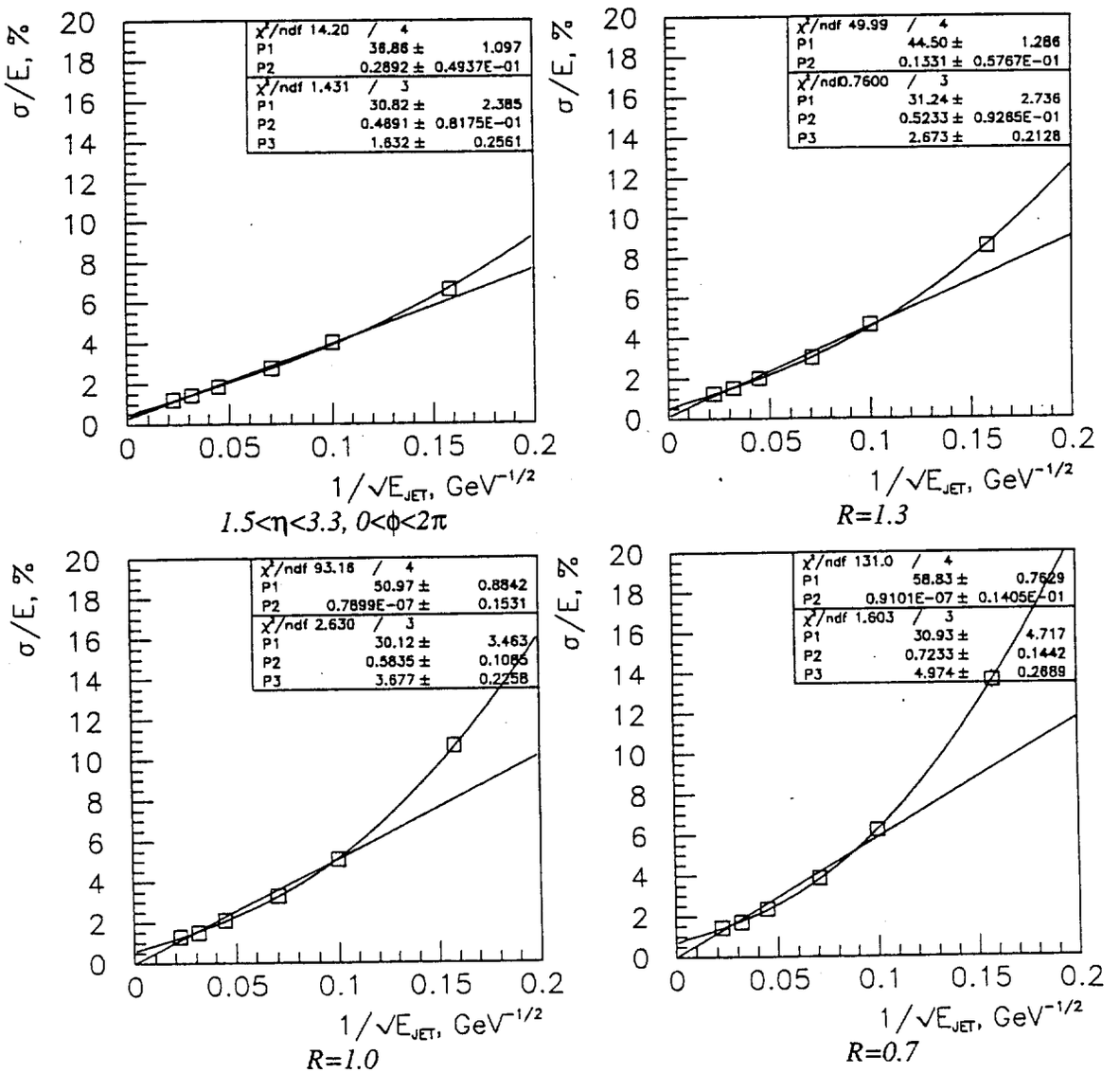


Figure 8: The energy dependence of the resolution for the configuration with a preshower (after three parameter minimization).

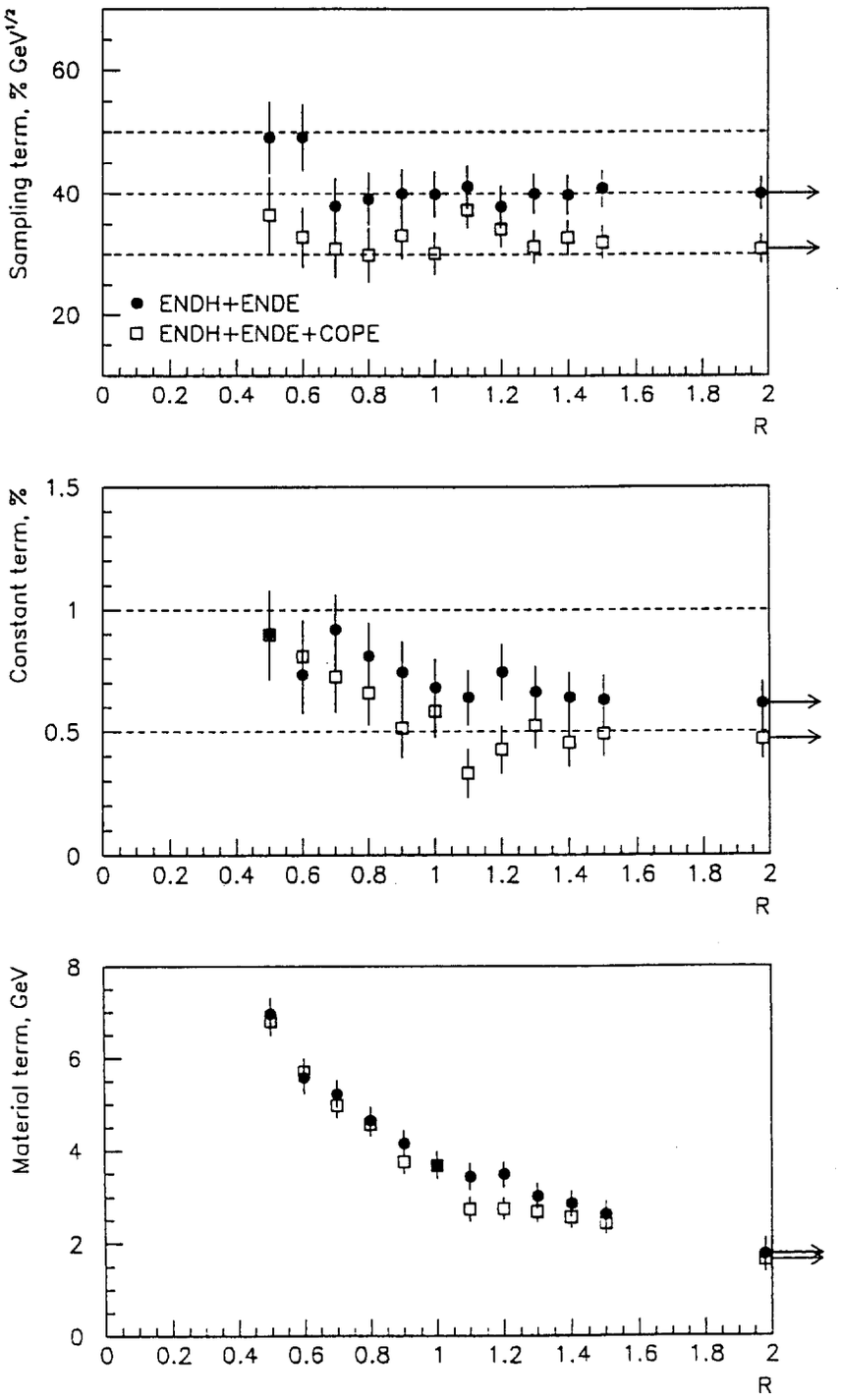


Figure 9: The dependence of the sampling, constant and material terms on the jet cone size considered. Points with arrows correspond to the total end-cap volume.